Experimental Astronomy (2024) 57:4
https://doi.org/10.1007/s10686-024-09925-z

RESEARCH

New Yarkovsky drift detections using astrometric observations of NEAs

Bedini Lisa[1] · **Tommei Giacomo**[2]

Received: 29 October 2023 / Accepted: 7 February 2024
© The Author(s) 2024

Abstract
The Yarkovsky drift represents the semi-major axis variation of a celestial body due to the Yarkovsky effect. This thermodynamic effect acts more significantly on bodies with a diameter between $\approx$ 10 m and $\approx$ 30 km. Therefore, the orbits of many minor bodies of the solar system are affected: knowing the value of the Yarkovsky drift can be crucial to accurately predict their positions, especially if the asteroids are Near Earth Asteroids (NEAs) and there may be a non-zero impact probability with the Earth. The direct computation of this effect is not easily achieved due to the scarce availability of NEAs physical information. Thus, the more promising method to estimate the Yarkovsky effect is through an orbital fit using seven parameters, the six orbital elements and a seventh parameter accounting for non-gravitational interactions. In this paper, we show the analysis of 1262 NEAs with Signal-to-Noise Ratio (SNR) greater or equal 2, of which 279 have the parameter S (absolute ratio between the Yarkovsky drift and its expected value) less than 1.5 and are therefore more reliable. Among these, 91 are not present in the literature, thus represent new Yarkovsky drift detections. Furthermore, we used our results to estimate the ratio of the retrograde over prograde rotators and to validate the dependence of the Yarkovsky drift from the diameter, da/dt $\approx D^{-1}$.

Keywords Asteroids · Yarkovsky effect · Orbit determination

1 Introduction

Studying the long term orbital evolution of a small body is quite a difficult task because of multiple planetary encounters and non-gravitational forces. However, the precise

Bedini Lisa and Tommei Giacomo contributed equally to this work

✉ Tommei Giacomo
giacomo.tommei@unipi.it

[1] Space Dynamics Services srl, Via Mario Giuntini 63, Navacchio di Cascina 56023, Pisa, Italy

[2] Department of Mathematics, University of Pisa, Largo B. Pontecorvo 5, Pisa 56127, Italy

Published online: 26 February 2024

computation and propagation of an asteroid orbit is essential, not only for scientific purpose, but also for planetary defense [1].

The Yarkovsky effect is a non-gravitational thermodynamic force based on the process of absorption and non-instantaneous re-emission of radiation by a rotating body. The need to include this effect in the orbit determination process came from some inconsistencies between the predictions of the asteroid classical model and the observations, especially regarding the delivery of asteroids into inner orbits, [2], with a particular interest in Near Earth Asteroids (NEAs). In fact, the classical model, see [3–6] and [7, 8], stated that collisions and gravitational interactions were the only means to inject asteroids into the strong resonances that were known to cause a drift of the asteroids toward the inner solar system. The drift would then make possible close approaches with the planets that could result in a collision event or in the injection on a stable orbit. The following list, from [9] and [10], presents four predictions of the classical model, which were not supported by the observations. This circumstance hinted to another kind of interaction affecting the orbital evolution of the asteroids in the Main Belt, other than collisions and gravitational force.

- Given that a typical lifetime for an asteroid in a strong resonance is of a few million years, we expect an abundance of cosmic-ray exposure (CRE) ages of a few million years for meteorites and NEAs; what is observed though, is that most of the meteorites have a CRE age of more than 10 million years. Some iron meteorites have CRE ages between 0.1 and 1 billion years.
- Collisions are the only mean to deliver ejecta into chaotic resonances and the NEA population of kilometer-size bodies is expected to be in steady state; this population presents various taxonomic types, but it is mainly composed of asteroids from inner and central Main Belt. Therefore, there must be several asteroid families, which are structures of asteroids resulting from a collision event, of different taxonomic type in those regions. Furthermore, the kilometer-sized NEAs distribution should be as steep as that of 'fresh ejecta'. This latter prediction is contradicted by the rather shallow size distribution of these NEAs, while the former is contradicted by the fact that there are a few families in these regions of the Main Belt and fewer still near a strong resonance.
- Due to a collision event, the size-velocity distribution should be determined by a weak formulation of the energy equipartition principle. These results are in disagreement with the hydrocode simulations, which suggest a smaller peak velocity, but are in agreement with the values inferred from the orbital positions of asteroid family members. Hydrocode models could not be complete, but they successfully predicted a wide dimension-range of laboratory impact and explosions experiments.
- The spin rate distribution of the asteroids resulting from a collision should be approximately a Maxwellian distribution, to the zeroth order. Instead, the spin rate distribution for small asteroids ($D < 10$ km) has an excess of fast and slow rotators compared to the expected distribution.

These inconsistencies can be removed by taking into account the Yarkovsky effect and its rotational variant, the YORP effect [10], for asteroids with a diameter between

approximately 10 m and 20−30 km . The Yarkovsky effect mainly causes a semi-major axis drift with typical values of $da/dt \simeq 10^{-4} - 10^{-3}$ AU My^{-1} for sub-kilometre NEAs.

The name of the effect comes from Ivan Osipovich Yarkovsky (1844 - 1902): he was a Russian engineer who published a pamphlet in 1901 about how the delay from absorption to re-emission of thermal radiation could produce the transverse acceleration necessary to counterbalance the drag caused by ether. Of course nowadays we know there is no ether, so Yarkovsky's conclusions and calculations are not to be taken in consideration other than for historical reasons, but the idea of such thermal effect was later rekindled. In fact, the Estonian astronomer Ernst Öpik in 1951, [11], brought this idea in Europe and almost at the same time Radzievskii (1952, [12]) published in Russia similar ideas developed with his collaborators. So the 1950s represented the starting point for the Yarkovsky effect theory. This theory was continuously developed and peaked in the 1990s thanks to the work of Rubincam, Bottke and Farinella amongst many others. An important milestone was the understanding that the drift affecting the LAGEOS1 and other artificial satellites was indeed caused by the Yarkovsky effect [13].

Concerning the dynamics of NEAs, the Yarkovsky effect was first predicted by [14] for the asteroid (6489) Golevka and discovered in 2003 thanks to the radar ranging of that object [15].

From 2008, thanks to the improvement in the accuracy of the observational process, many scientists published catalogs of Yarkovsky effect detections: [16–22]. As the observational tools improve and the quality of the observations increases, a noticeable example is the Gaia DR3 [23], the catalog of objects with a detectable effect is bound to grow. It is legitimate to think that it is now superfluous to continue publishing these results in scientific peer-reviewed papers, limiting ourselves to updating the existing databases; however we believe that a comparison and a debate on the methods, the algorithms and the software used (often different between the various research groups) can always be productive, and it is right that this comparison is made available to the entire scientific community. Moreover the discussion could give rise to new investigations. For these reasons in this work we present our updated results, compared to the latest published catalogues, [20–22] and to the JPL Small Body Orbits & Ephemerides database.[1]

The paper is organized as follows. In Section 2 we briefly describe the mathematical modeling of the Yarkovsky effect and its computation starting from the heat equation; then we show the orbit determination methods used to perform the detection of the effect. In Section 3 we show the results obtained using the OrbFit software[2] and we discuss them in relation with the ones already known. Section 4 deals with the analysis of some interesting objects, while in Section 5 we discuss about the prograde and retrograde NEAs and the known dependence of the semi-major axis variation on diameter. In the last section we draw some conclusions.

[1] https://ssd.jpl.nasa.gov/sb/orbits.html

[2] http://adams.dm.unipi.it/orbfit/

2 Methods

2.1 Yarkovsky model

It is known that the hotter the surface of a body is, the more photons it will emit, so the differences of temperature across the surface of an asteroid may cause a resulting momentum carried away by photons in a specific direction. Each photon carries away a momentum equal to $|\mathrm{p}| = E/c$, where E is the photon energy and c is the speed of light, directed along its path; the sum of each of these momenta is what causes the recoil applied to the asteroid [9]. This recoil force produces a change mainly in the semi-major axis of the body over a large time span and has two components: the diurnal and the seasonal component.

The diurnal component is caused by the rotation of the asteroid around its spin axis: the re-emission of the absorbed radiation is delayed because of the non-zero thermal inertia, therefore, the recoil due to the re-emission has both a radial and a transverse component and it does not perfectly lie on the Sun-asteroid line.

The first order variation of the semi-major axis a can be written, following [24], as:

$$\left\langle \frac{da}{dt} \right\rangle = -\frac{8}{9}\frac{\alpha}{n}\frac{\Phi}{} W(R_\omega, \Theta_\omega) \cos\gamma \ . \tag{1}$$

The brackets represent the average value over a rotation period around the spin axis; $\alpha = 1 - A$, with A being the Bond albedo; $\Phi = \pi R^2 F/(mc) \propto 1/R$ is the radiation pressure coefficient; R is the radius of the object; F is the incoming flux; m is the object mass; n is the orbital mean motion; γ is the spin axis obliquity. The generalized term $W(R_\nu, \Theta_\nu)$ is a function of the thermal properties of the object and of the general frequency ν, which is the rotation frequency ω in the case of the diurnal component:

$$W(R_\nu, \Theta_\nu) = -\frac{\kappa_1(R_\nu)\,\Theta_\nu}{1 + 2\,\kappa_2(R_\nu)\,\Theta_\nu + \kappa_3(R_\nu)\,\Theta_\nu^2} \tag{2}$$

The terms κ_i are analytic functions of $R_\nu = R/\sqrt{K/(\rho\, C\, \nu)} = R/\ell_\nu$; the term ℓ_ν depends on the conductivity K of the body, its surface heat capacity C, its surface density ρ and on ν, the frequency of the irradiation of the surface. Physically, ℓ_ν represents a characteristic scale length which provides an estimate for the penetration depth of the thermal wave. The thermal parameter $\Theta_\nu = \Gamma\sqrt{\nu}/(\epsilon\,\sigma\,T_{sub}^3)$ depends on the surface thermal inertia $\Gamma = \sqrt{K\,\rho\,C}$, the thermal emissivity of the surface ϵ, the Stefan-Boltzmann constant σ and on the subsolar temperature defined by the relation $\epsilon\,\sigma\,T_{sub}^4 = \alpha\,F$.

Given that $W(R_\nu, \Theta_\nu)$ is negative, because thermal re-emission happens some time after the absorption, (1) explains that the semi-major axis of an asteroid with $\cos\gamma > 0$ increases with time, while if $\cos\gamma < 0$ the semi-major axis decreases. Finally, if $\cos\gamma = 0$, the diurnal component vanishes because the portion of the surface facing the Sun does not change in a rotation, so the recoil is radial. If the body is a very fast rotator, the temperature differences of the surface tend to smooth out, thus the re-emission become isotropic and there is no net momentum due to the emission of the photons [10]. The diurnal component become negligible even in the case of an

asteroid with zero rotation, because the recoil is radial thus it has not a transverse component.

The seasonal component is due to the revolution of the asteroid around the Sun and it is most effective when the spin axis lies on the orbital plane; in this case the important frequency is the orbital mean motion n. The first order variation of the semi-major axis can be written, following [24], as:

$$\left\langle \frac{da}{dt} \right\rangle = \frac{4\alpha}{9} \frac{\Phi}{n} W(R_n, \Theta_n) \sin^2 \gamma \tag{3}$$

where the parameters have the same meaning of those described for the diurnal component. The function $W(R_n, \Theta_n)$ has the same form of (2), substituting the general frequency ν for the mean motion n. As already mentioned, the variation of the semi-major axis in time is always negative and vanishes when the spin axis is perpendicular to the orbital plane, because in that case there is not one hemisphere more illuminated than the other during the revolution.

In general, the diurnal component dominates over the seasonal component, therefore we can assume, as a first-order approximation, that if an asteroid has a prograde rotation, its semi-major axis will increase [14].

2.2 Dynamical model

Given that the magnitude of the Yarkovsky drift for a sub-kilometer NEA is of the order of $10^{-15} - 10^{-13}$ AU d^{-2} [20], we have to choose the dynamical model for Orbit Determination (OD) process accordingly, including all the relevant terms; for this reason our dynamical model includes the Sun, the planets, Pluto and the 17 more massive asteroids. The Yarkovsky effect is primarily modeled as a transverse acceleration

$$\mathbf{a}_t = A_2 \, g(r) \hat{t}$$

where A_2 is a parameter to estimate in the OD procedure together with the orbital elements. The function $g(r)$ can be modeled as a power law

$$g(r) = (r_0/r)^d \ ,$$

where r_0 is a normalizing factor and the exponent is bounded: $0.5 \leq d \leq 3.5$. In order to compute the mean value for the semi-major axis drift, we integrate over an orbital period T and operate a Taylor expansion:

$$\left\langle \frac{da}{dt} \right\rangle = \frac{2A_2 \, (1 - e^2)}{n} \left(\frac{r_0}{a(1 - e^2)} \right)^d J(e, d) \tag{4}$$

where

$$J(e, d) = \sum_{k=0}^{\infty} \binom{d - 1}{2k} \binom{2k}{k} \frac{1}{2^{2k}} e^{2k} \ . \tag{5}$$

Even though d depends on the thermal properties of the object and cannot generally be computed, it was empirically found that most NEAs[3] have $2 \leq d \leq 3$. Furthermore, the semi-major drift does not depend strongly on the d value [18]. Following [20], we assume $d = 2$ for every asteroid except for Bennu, of which we have more knowledge of its thermal properties, so $d = 2.25$, [25]. The function $J(e, d)$ is finite if d is an integer and in particular $J(e, 2) = 1$. Once the A_2 parameter is estimated, the semi-major axis drift can be inferred as [18]:

$$\frac{da}{dt} = \frac{2a\sqrt{1-e^2}}{n\,r} A_2\, g(r) \tag{6}$$

where a, e and n are the usual semi-major axis, eccentricity and mean motion respectively, and r is the heliocentric distance.

Regarding the OD procedure, a preliminary orbit is computed with a set of initial conditions at an epoch t_0, $\mathbf{y}(t_0) = \mathbf{y}_0$. In this case, we used the spatial coordinates downloaded from the NEODyS website.[4]

The preliminary orbit is refined applying the Least Squares (LS) principle. Following a classical approach (see, for instance, [26]), the non-linear LS fit leads to compute a set of parameters $\mathbf{u}$ (the orbital elements and the A_2 parameter in our case) which minimizes the following target function:

$$Q(\mathbf{u}) = \frac{1}{m}\boldsymbol{\xi}^T(\mathbf{u}) W \boldsymbol{\xi}(\mathbf{u}) = \frac{1}{m}\sum_{i=1}^{m} w_i \xi_i^2(\mathbf{u}), \tag{7}$$

where m is the number of observations and $\boldsymbol{\xi}(\mathbf{u}) = \mathcal{O} - \mathcal{C}(\mathbf{u})$ is the vector of *residuals*, difference between the observed quantities $\mathcal{O}$ and the predicted ones $\mathcal{C}(\mathbf{u})$, computed following suitable mathematical models and assumptions; in our case, $\mathcal{O}$ are astrometric observations. Finally, w_i is the weight associated to the i-th observation. Other information required to such orbit propagations are supposed to be known: positions and velocities of the other planets of the solar system are obtained from the JPL ephemerides DE441 [27], while the rotation of the Earth is provided by the interpolation table made public by the International Earth Rotation Service (IERS)[5].

The procedure to compute $\mathbf{u}^*$, the set of parameters which minimizes $Q(\mathbf{u})$, is based on a modified Newton's method known in the literature as *differential corrections method*; all the details can be found in [26] - Chap.5. Let us define:

$$B = \frac{\partial \boldsymbol{\xi}}{\partial \mathbf{u}}(\mathbf{u}), \qquad C = B^T W B,$$

which are called the *design matrix* and the *normal matrix*, respectively. Then, the correction:

$$\Delta\mathbf{u} = C^{-1} D \quad \text{with } D = -B^T W \boldsymbol{\xi}$$

[3] Unless they have a very large rotational period or a remarkably large or small thermal inertia.

[4] https://newton.spacedys.com/neodys/

[5] IERS: http://www.iers.org

is applied iteratively until either Q does not change meaningfully from one iteration to the other or $\Delta\mathbf{u}$ becomes smaller than a given tolerance. Introducing the inverse of the normal matrix, $\Gamma = C^{-1}$, we always adopt the probabilistic interpretation of Γ as the *covariance matrix* of the vector $\mathbf{u}$, considered as a multivariate Gaussian distribution with mean $\mathbf{u}^*$ in the space of parameters.

2.3 Yarkovsky expected value

In the analysis we performed it has been important to compute an expected value of the Yarkovsky drift because the model described above does not distinguish the Yarkovsky effect from other effects that can alter the orbit of an asteroid. Therefore, if the expected value of the Yarkovsky drift is significantly different with respect to the computed one, a possible cause may be that the asteroid orbit is influenced also by other interactions than the expected ones.

The expected value of the Yarkovsky drift [18] is computed using the scaling formula from [28], considering the asteroid (101955) Bennu as a reference. This asteroid is one of the most studied NEAs and its estimate for the Yarkovsky drift has a Signal-to-Noise Ratio (SNR) $\approx$ 1400 thanks to the results collected by the OSIRIS-REx mission, [29]. The scaling relation is:

$$\left(\frac{da}{dt}\right)_{exp} = \left(\frac{da}{dt}\right)_{B} \times \frac{\sqrt{a_B}(1-e_B^2)}{\sqrt{a}(1-e^2)} \frac{D_B}{D} \frac{\rho_B}{\rho} \frac{\cos\gamma}{\cos\gamma_B} \frac{1-A}{1-A_B} \tag{8}$$

The suffix B refers to the asteroid (101955) Bennu, see Table 1. There are other parameters influencing the strength of the Yarkovsky force and therefore the drift it causes, in particular the surface thermal conductivity and the thermal inertia. Due to the fact that the data for these parameters are not available, they are not explicitly written in the (8).

The orbital parameters a and e are always available for the asteroids considered in this work, but this is not true for the physical parameters and the obliquity. In

Table 1 Orbital and physical parameters of (101955) Bennu

(101955) Bennu - Parameters		
a	$1.13\ (\pm 1.97 \times 10^{-10})$	AU
e	$0.20\ (\pm 6.97 \times 10^{-11})$	
ρ	$1.26\ (\pm 0.07)$	g cm^{-3}
p_v	$0.044\ (\pm 0.002)$	
D	$0.482\ (\pm 0.3)$	km
γ	$178\ (\pm 4)$	deg
da/dt	$-19.0\ (\pm 0.1) \times 10^{-4}$	AU Myr^{-1}

The value of the semi-major axis a, eccentricity e, density ρ, geometric albedo p_v and diameter D are from the JPL-SBDB online service, while the value of the obliquity γ and of the Yarkovsky drift da/dt are from [30]

fact, many NEAs do not have estimates for D, ρ, γ and A, therefore we made some approximations following [20]. In general, the obliquity is not given and because its value cannot be estimated using other variables, its contribution to the drift is maximized, assuming $\cos\gamma = 1$. If the diameter is not given, we computed it using the relation from [18]:

$$D(H, p_v) = \frac{1329\,\mathrm{km}\,10^{(-0.2\,H)}}{\sqrt{p_v}} \tag{9}$$

where H is the absolute magnitude and p_v is the geometric albedo. Generally, the Bond albedo is not explicitly given, but it is related to the geometric albedo p_v and to the parameter G [31]: $A = p_v\,(0.290 + 0.684\,G)$. If the parameter G is not given, its value is put equal to 0.15 [31]. Regarding the geometric albedo, if it is not given, the arithmetic mean value of p_v can be used. We computed this value considering the NEAs for which the geometric albedo was given and found a mean value of 0.172. If the density is not given, a method to evaluate it consists on using an asteroid of known density ρ and applying the scaling relation $\rho_s = \rho\,(1 - \mathcal{P})$. Here, $\mathcal{P}$ is the porosity factor and the scaled density ρ_s corresponds to that of an asteroid with a diameter of 1 km. Therefore, the ρ_s value is computed from a known density and porosity of another asteroid, best if the taxonomic class is the same.

We updated the porosity factors for the most populated taxonomic classes, the C and S class. We chose, applying the criterion of highest SNR, the densities of (10) Hygiea and (15) Eunomia as ρ and the ones of (253) Mathilde and (433) Eros as ρ_s. Thus, we computed the porosities using the inverse of the relation, see Table 2. For the B class we used the porosity of Bennu, 0.40, [25], while for the other classes or for the unknown class we computed a mean scaled density of $1.72\,g\,cm^{-3}$ and a mean porosity of 35.3 %.

3 Analysis and results

In this section we are going to analyze the results obtained: we will show our output and we will perform a comparison with existing databases ([20–22] and the SBDB).

Table 2 Asteroids used to compute the scaled density

Name	Tax. class	Diameter [km]	Density [g cm^{-3}]	porosity
(10) Hygiea	C	407.12 ± 6.8	2.19 ± 0.42	–
(253) Mathilde	Cb	52.8 ± 2.6	1.3 ± 0.2	41%
(15) Eunomia	S	231.69 ± 2.23	3.54 ± 0.20	–
(433) Eros	S	16.84 ± 0.06	2.67 ± 0.03	25%

The relation to compute the scaled density is $\rho_{s,i} = (1 - \mathcal{P}_i)\,\rho_i$, where i refers to the taxonomic class. The first line in each block refers the large asteroid considered to scale the density for a certain taxonomic class and supplies the value ρ_i. The second line refers to the asteroid used to compute the porosity of the taxonomic class and the scaled density, using the value $\mathcal{P}_i$. The data are from SBDB

The initial selection of the asteroids was performed filtering the objects in the NEODyS database, on the 13th of March 2023, taking the ones with the arc type ≥ 10. The arc type is an integer value which represents the number of chronologically consecutive Too Short Arcs (TSAs), see [32]. The threshold value is chosen empirically, to be sure to include all the objects for which the seven parameters fit could be computed, while discarding the ones for which this procedure could result in spurious values or errors. To give an idea, the arc type of a one-nighter is typically 2 and the observations are not sufficient to obtain reasonable results from a seven parameters orbit fit.

The initial set contained 17 629 objects and we have performed the seven parameters OD for all of them, using the OrbFit software. We employed the VFCC17 weighting, [33], and the FCCT14 error model, [34]. The fit failed to produce the non-gravitational parameter for 47 NEAs. The number of failures is negligible with respect to the total number of NEAs in the dataset, but it is not zero. This gives us the certainty to have included the majority of asteroids for which is possible to compute the seven parameters fit while minimizing the computation resources and time wasted (Fig. 1).

The fact that the fit did not fail is not a guarantee that the seventh parameter values have a physical meaning. Therefore, we decided to keep in the database only the NEAs presenting a Yarkovsky drift SNR$\geq$ 2. The dataset counts 1262 asteroids and it is available as online material.

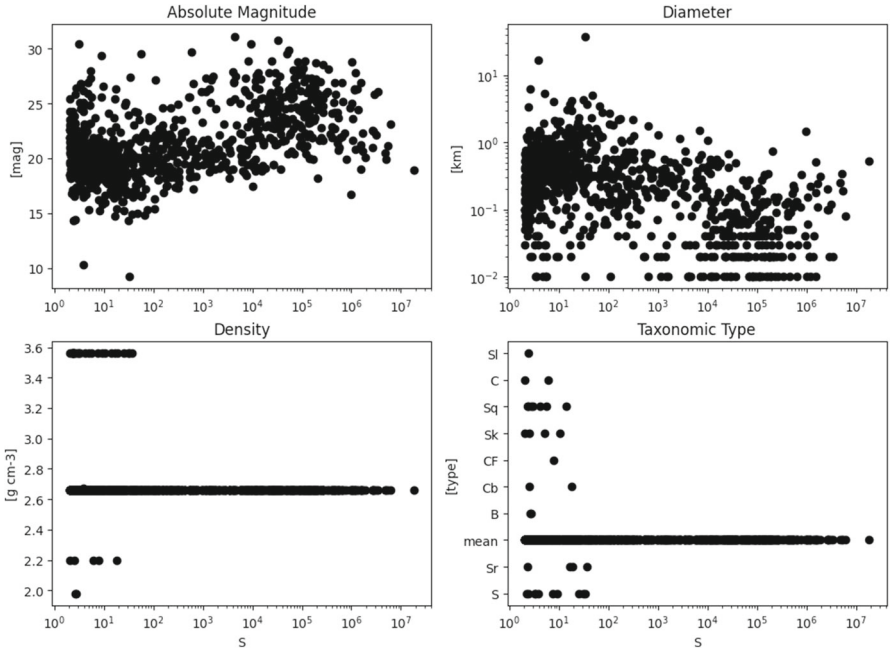

Fig. 1 Four plots showing the distribution of a few physical parameters for the Yarkovsky drifts with $S \geq 2$. The considered parameters are, from left to right and from top to bottom: absolute magnitude, diameter, density and taxonomic type. For each plot, the x-axis represents the S parameter

For each of these NEAs we computed the S parameter, see [18], defined as the absolute ratio between the Yarkovsky drift and its expected value, computed using (8). Given that the physical and thermal properties of an asteroid are seldom available, we computed the expected value using the approximations described in Section 2.3. The distribution of the S parameter is displayed in Fig. 2. Looking at this histogram, we see that for many asteroids $S \geq 2$, the maximum being $\approx 2 \times 10^7$.

We performed a preliminary analysis to find an explanation to the fact that 874 measurements have $SNR \geq 2$ and $S \geq 2$. We qualitatively studied the distribution of four parameters as a function of S, Fig. 1: absolute magnitude, diameter, density and taxonomic type.

- The absolute magnitude and diameter distributions suggest that the sample is composed of NEAs with a size ≤ 10 km;
- the density distribution shows that for 841 NEAs this information was not given, so the mean density value was used. The taxonomic type distribution confirms this trend.

Therefore, it seems that this sample is composed of small asteroids with no physical characterization. This combination can alter the S value because small asteroids may be subject to other non-gravitational effects. Moreover, the uncertainty on the density and on the other physical parameters plays an important role. In order to fully understand this scenario would require a thorough analysis, which is out of the scope of this paper.

In general, if the S parameter is far from one, it means that the model used to compute the expected value do not reflect the actual situation. For example, if $S << 1$ the obliquity of the asteroid may be $\approx 90°$, while if $S >> 1$ the albedo may be larger than expected (see 2008 BD) or the thermal properties may be significantly different with respect to the ones of Bennu. Another reason for a high value of S may be a high

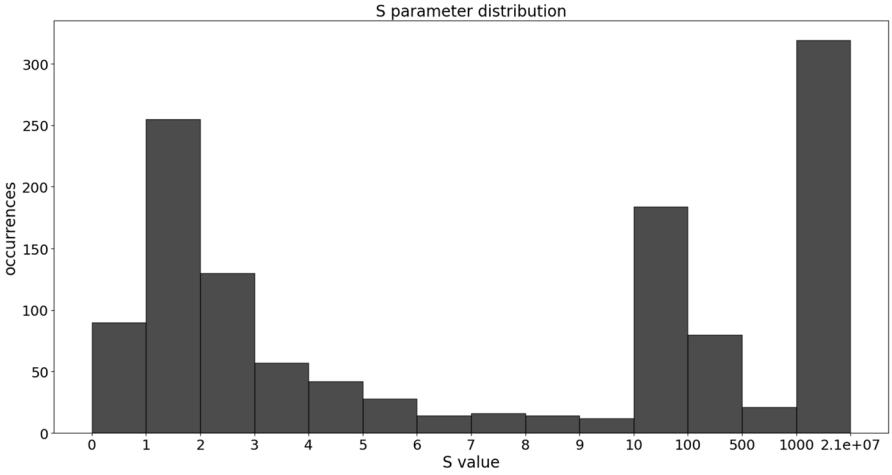

Fig. 2 Frequency histogram of the S parameter values. Note that the bins are not equally spaced because the more interesting values are the smaller ones. The last bin has the maximum computed value of S as upper limit

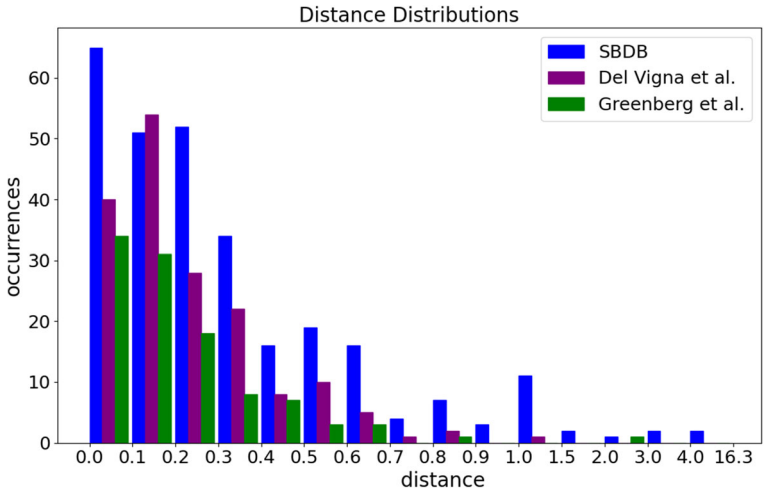

Fig. 3 Frequency histogram of the distance computed between the data from this work and that from SBDB (blue), [20] (purple), [21] (green). Note that the bin intervals are not equally spaced for a better readability. The matches with [22] are not shown in the histogram due to their small number

value of the computed Yarkovsky drift, which may be due to erroneous astrometry, see [19].

Therefore, it is clear that the threshold on the SNR is not sufficient to claim a detection. Thus, we applied a selecting criterion on the S parameter, considering the detection valid if $S \leq 1.5$, [19], and $SN \geq 2$. The criterion on S rejected 983 objects, so the dataset counts 279 Yarkovsky detections.

3.1 Comparison and validation

We compared our results with those from [20–22] and the SBDB.

In order to check whether or not two values are comparable (in our case, we are comparing two values of Yarkovsky drift computed by us and different authors), we computed the distance D as follows:

$$D^2 = \frac{(a-b)^2}{\sigma_a^2 + \sigma_b^2} \tag{10}$$

where $a \pm \sigma_a$ and $b \pm \sigma_b$ are two measurements. We define a sort of new value $(a-b)^2$ and we weight it with its variance, given by the sum of the variances of a and b. Assuming a sort of Gaussian statistics, we consider the measurements comparable if $D \leq 3$.

Regarding the data from [20] and [21], we found respectively 109 among a total of 111 and 171 among 255 that match with our data. As one can see in Fig. 3, all matches have a distance ≤ 3, so we consider them comparable. There are 2 NEAs[6] from the

[6] 162142 and 471240.

Table 3 Comparison with [22] data

Asteroid	Distance
1036	0.988
1685	0.890
1864	0.384
2062	2.917
2063	1.228
2100	0.014
3103	0.166
3200	1.060

Asteroid designation and distance between the Yarkovsky drift values computed by [22] and the ones from this work. Every match presents a distance ≤ 3, thus our results are comparable with those from [22]

Del Vigna dataset that are not included in our dataset because of the threshold on the SNR. The same is true for the 84 NEAs[7] from the Greenberg dataset. The fact that there are so many mismatch with the Greenberg dataset is due to the fact that their selecting criteria do not explicitly take the SNR into account.

Regarding the data from [22], they included the orbital information from the Gaia DR2 and computed the Yarkovsky drift value for 42 asteroids, both NEAs and from the Main Belt. Among these, 8 are present in our dataset, as shown in Table 3. Given that the distance for those NEAs is ≤ 3, we consider our data comparable. There are 34 asteroids in the Dziadura dataset that are not included in our dataset: 8 of these are asteroids from the Main Belt[8] and the remaining 26 NEAs[9] are excluded because of the SNR threshold.

Regarding SBDB, this online database contains 311 NEAs with an estimate of the A_2 parameter.[10] We found a match with 285 of these and as one can see in Fig. 3, the matches have a distance ≤ 3 except for 523599, 2006 RH120 and 2015 TC25. These inconsistencies seem to arise from a different set of measurements used to compute the orbit. Furthermore, the second and third have orbits comparable to that of the Earth and this could cause issues with our orbit determination software. See [19] for an accurate description of 2006 RH120. There are 26 NEAs in the SBDB dataset that are not included in our dataset: 2008 WT62 was excluded because it has an arc

[7] 719, 1620, 1866, 1915, 1916, 2061, 2201, 2202, 3753, 4197, 4769, 5011, 5131, 5189, 5693, 5869, 6239, 7482, 7822, 7889, 8176, 9162, 9856, 10563, 11398, 11405, 11500, 15745, 17511, 31221, 52387, 65690, 65706, 65733, 66146, 66391, 87684, 88959, 96590, 136617, 136993, 137805, 141018, 141498, 161999, 162142, 162463, 162483, 162567, 162882, 163081, 164202, 190491, 190758, 215442, 217628, 230549, 240320, 243025, 244670, 249886, 252399, 276033, 302169, 326302, 333889, 363116, 433953, 438661, 450293, 452389, 455594, 461353, 461852, 467336, 474574, 488453, 488789, 494658, 495829, 523586, 523595, 2004 BG41 and 2004 SC56.

[8] 244, 1103, 1139, 1747, 2629, 3800, 5427 and 6618.

[9] 1620, 1866, 1943, 3554, 3753, 4769, 4953, 5381, 7889, 10563, 12711, 66146, 66391, 68216, 85818, 86667, 87684, 88710, 96590, 105140, 137805, 137925, 154555, 163693, 163899 and 164121.

[10] At May, 2023

type = 7, 2020 FW6 was not included because its discovery MPEC was published after the selection of the NEAs for this work; the remaining 24 were excluded by the SNR threshold. These checks were performed considering our complete dataset, applying only the SNR threshold. This is to verify the overall consistency of the non-gravitational fit parameter. Considering also the threshold on S, we find 162 objects that have a Yarkovsky estimate but $S > 1.5$. This is due to the fact that [21] and the SBDB do not apply the same criteria. Regarding the data of [20], their threshold was higher and they used different values to compute the expected drift.

3.2 New results

Our dataset shows 91 Yarkovsky drift values not present in the literature, of which 26 have a SNR ≥ 3. In Table 4 these new detections are displayed, together with the information about the Yarkovsky drift (computed and expected), the SNR and the S parameter.

As shown in the table, there are some asteroids with $S \leq 0.5$, like 2017 UJ5, 2006 AN and 2013 BO27. These are generally small asteroids, $H \approx 22 - 24$ mag, and a lower computed Yarkovsky drift may be due to a non-significant difference in the thermodynamic properties with respect to Bennu, a peculiar orbital dynamics, like a high rotation or high obliquity, and/or erroneous astrometry. (5797) Bivoj is the bigger of these asteroids, $H = 18.89$ mag and the discrepancy between the expected and the computed drift may be due to its high rotation period ≈ 2.706 h, [35].

4 Specific cases

In this section we discuss some particular and interesting objects.

4.1 (99942) Apophis

It is an interesting asteroid that, much as (4179) Toutatis, has a tumbling motion. This means that it does not have a preferred rotation axis and therefore, a Yarkovsky effect estimate is more difficult to obtain. For this reason this asteroid was considered of marginal significance by [20], considering also the low SN ratio computed - 1.80. The result obtained in this work is greatly improved thanks to the new optical and radar measurements. In fact, the optical observations during the years 2020-2021 account for the $\approx 43\%$ of the entirety of the observations and the number of radar observations was increased by four on March, 2021. The increase of the number of observations led to a remarkable increase of the SN ratio, which is 117.82. Despite this, for this asteroid $S = 1.58$ so it was rejected by the second criterion. This may be due to the fact that the Bennu scaling is more accurate if an asteroid has physical properties similar to Bennu. In fact, if we compare the Yarkovsky drift we found, $da/dt = (-13.31 \pm 0.11) \times 10^{-4}$ AU Myr^{-1}, with the one computed in [36], using more accurate physical parameters values, we see that the two are in agreement.

Similarly, our value is in agreement with the results from [37] and [38], respectively the distance is of 0.99 and 0.03.

4.2 (4179) Toutatis

It is the asteroid aforementioned, known for its tumbling motion. Unfortunately, there are no new radar observations, but, throughout 2020-2022 the number of optical observations is increased, thus the SNR increased from 7.17 [21] to 9.12. However, the value of the SNR may actually be lower due to the fact that this asteroid crosses the Main Belt and this increases the uncertainty of the perturbing asteroid masses, [18]. Analogously to 99942, 4179 was rejected because of the S parameter value, but, given the peculiarities of this object, we can compare our detection with direct Yarkovsky drift computations in the literature, like the one in [39]. They computed the average Yarkovsky drift as function of the surface conductivity, finding the range $\approx [-0.35, -1.50] \times 10^{-4}$AU Myr^{-1}. The S parameter would still be slightly over the threshold, $S \approx 1.75$, but this may be due to unmodeled perturbations or to the peculiar shape and motion of the asteroid.

4.3 (483656) 2005 ES70

It is a remarkable asteroid because of its high Yarkovsky drift value, $(-89.56 \pm 3.28) \times 10^{-4}$ AU/Myr, and a high SN ratio, 27.3. This is due to the fact that it is a small asteroid, with a diameter of only 0.06 km, therefore the Yarkovsky effect is more efficient than in other cases. The results are confirmed by [20, 21], SBDB and $S = 0.96$.

4.4 2008 DB

It is a relatively recently discovered NEA, which presents a large, in absolute value, Yarkovsky drift and a SN> 3, $(-483 \pm 57) \times 10^{-4}$ AU/Myr and 8.5 respectively. This asteroid is similar to *2009 BD*, analyzed by [21]. *2008 DB* is also a small asteroid, with a diameter of 0.02 km and thus the Yarkovsky effect is more efficient. This and a favorable surface-to-mass ratio, can make for a high secular change in the semi-major axis. Furthermore, the albedo could be large, as for *2009 BD*, [40], thus resulting in an high value of Yarkovsky drift. In fact, the expected Yarkovsky drift is 164.86×10^{-4} AU/Myr, but $S = 2.63$ so more information are needed to claim the detection.

4.5 (185851) 2000 DP107

It is a binary asteroid [41] present in the Greenberg and the SBDB dataset. Thanks to the new optical observations in 2019-2022, the SN ratio of its Yarkovsky drift value increased from 2.37 to 15.22 and $S = 0.44$. Binary asteroids with a detected Yarkovsky drift can be useful to check the theory of the binary Yarkovsky effect.

4.6 (39565) 1992 SL

It is an asteroid cited by [20] because of the particularity of the first recorded observation, which is a single measurement in 1950. Follows then a gap until 1992 but after that the NEA has been observed regularly, until 2023. Unfortunately, the actual arc length used to compute the orbit is 1992-2023, because the 1950 observation is automatically discarded by our system due to the high residuals. In this case, a remeasure of this observation might have a large impact for the Yarkovsky drift computation, given the significant increase of the arc length. The SNR is 7.68 but $S = 2.93$ so more information are needed to claim the detection.

4.7 2021 GM1

The interest in this asteroid comes from its high Yarkovsky drift value of $(-4.72 \times 10^3 \pm 488.33) \times 10^{-4}$ AU Myr^{-1} combined with an expected value of $1.34 \times 10^3 \times 10^{-4}$ AU Myr^{-1}: the value of the S parameter is 3.15. This high expected drift could be due to a combination of physical and dynamical factors: 2021 GM1 is a small Aten asteroid ($H = 30.4$), with low inclination and eccentricity. It would be interesting to have more information about this object to see if such high expected drift is confirmed.

5 Additional results

5.1 Prograde and retrograde NEAs

The relative abundance between prograde and retrograde rotators can be inferred using our dataset and compared with existing models in order to validate our results.

In fact, assuming that the Yarkovsky effect is predominant over other secular effects and the diurnal component is predominant over the seasonal one, the prograde rotation results in a positive Yarkovsky drift while the drift is negative for a retrograde NEA. In particular, the number of retrograde rotators is expected to be greater than the number of prograde ones. This is explained considering that resonances are the main mechanism that deliver asteroids from the main belt to inner orbits, with the Yarkovsky force feeding asteroids into these resonances (the direct injection via collisions can be neglected).

The ν_6 secular resonance is believed to have transported the $\approx 30\% - 37\%$ of NEAs from the inner part of the main belt [42]. Given its position, the asteroids reach it if their semi-major axis decreases, thus, if they are retrograde. The other remarkable resonances, like the 3 : 1, can be reached both by retrograde and prograde asteroids. Therefore, the expected ratio of the number of retrograde over prograde NEAs is $N_r/N_p \approx (1 + P_{\nu_6})/(1 - P_{\nu_6}) \approx 2 \pm 0.2$, where P_{ν_6} refers to the delivery efficiency of the ν_6 resonance.

In our detections, the number of retrograde rotators is 201, while the number of prograde ones is 78, thus the ratio is $N_r/N_p = 2.58$. Given that our data represents a finite sample of the NEAs population, we account for the sampling error as in [21]:

$\sigma_s = 0.35$. The value is within the confidence region of the expected ratio, although it is on the high end of the interval. This over-abundance of retrograde rotators could be due to a bias in the sample or to some approximation in the model.

5.2 Dependence on the diameter

As shown in (8), the semi-major axis drift has a dependence from the diameter which is approximately $da/dt \propto D^{-1}$. In particular, as shown in [43]:

$$\frac{da}{dt} \propto D^{-1} \frac{0.5\,\Theta_\nu}{1 + 2\,\Theta_\nu + 0.5\,\Theta_\nu^2} \tag{11}$$

where the relation makes use of (2). The thermal parameter Θ_ν peaks around 1.4 and therefore the previous relation can be approximated as [21]:

$$\frac{da}{dt} \propto D^{-1}\,\Theta_\nu^0 \propto D^{-1}\,. \tag{12}$$

Considering the double constrained dataset, the result of the fitting procedure is $da/dt \propto D^{-1.08\pm0.04}$, in agreement with the expectations. In Fig. 4 are displayed both the data and the least squares best fit.

6 Conclusions and further improvements

The Yarkovsky effect is fundamental in long-term dynamics of NEAs, and it is crucial to collect information in order to estimate the corresponding drift. Although dedicated physical observation campaigns of NEAs are being conducted and space missions to asteroids are underway and under study (e.g. Hera mission, [44]) the more effective method to estimate the Yarkovsky effect remains the OD from astrometric observations.

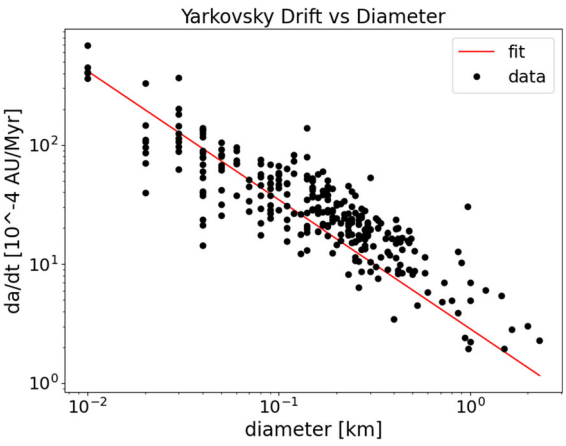

Fig. 4 Computed Yarkovsky drift as a function of the diameter, logarithmic scale. The dots refer to the data and the red line refers to the least squares fit

In this paper, using a seven parameters OD, we computed the Yarkovsky drift value for 1262 NEAs: 91 were new detections, of which 26 with a SNR ≥ 3.

In general, this new results can be seen as preliminary detections for future investigations. In fact, there are some NEAs, like 2017 UJ5 and 2006 AN, which have a low value of S and thus require a further investigation of their properties.

Furthermore, the detections are employed to validate two predictions of the Yarkovsky effect theory: the ratio of retrograde over prograde NEAs of $N_r/N_p \approx 2.58$ and the trend $da/dt \propto D^{-1.08\pm0.04}$.

Regarding the further improvements, it would be interesting to analyze the objects which have a high SNR but are rejected by the S parameter threshold and vice versa. This requires a study on possible orbit determination effects and physical characterization.

Appendix A: List of 91 new Yarkovsky drift detections

Table 4 These detections have $S \leq 1.5$ and SNR≥ 2

Asteroid	da/dt	$\sigma_{da/dt}$	SNR	$da/dt\|_{exp}$	S
1221	−2.23	0.68	3.28	3.52	0.63
5797	−3.47	1.63	2.13	8.94	0.39
6037	−8.77	3.12	2.81	9.2	0.95
11284	−4.81	2.26	2.13	4.73	1.02
26310	−8.41	2.95	2.85	7.85	1.07
65909	−13.35	4.69	2.85	12.07	1.11
68347	−20.08	7.89	2.54	14.15	1.42
152564	17.54	6.95	2.52	17.38	1.01
154300	−15.32	4.71	3.25	10.78	1.42
162422	−24.06	10.26	2.35	20.47	1.18
175729	−17.65	6.0	2.94	12.26	1.44
194006	−10.61	4.17	2.54	15.42	0.69
234145	−11.48	4.25	2.7	13.92	0.83
285179	−16.49	8.11	2.03	11.77	1.4
286079	−16.74	5.06	3.31	12.87	1.3
303450	22.57	9.32	2.42	19.76	1.14
311554	−11.97	5.04	2.37	12.55	0.95
360502	17.77	6.02	2.95	18.33	0.97
363067	−8.45	3.12	2.71	6.82	1.24
382406	−37.63	17.08	2.2	36.03	1.04
382875	26.8	11.97	2.24	24.78	1.08
390725	−22.46	9.99	2.25	16.38	1.37
401856	−13.52	3.89	3.47	15.02	0.9
410622	−18.55	7.21	2.57	22.29	0.83

Table 4 continued

Asteroid	da/dt	$\sigma_{da/dt}$	SNR	$da/dt\|_{exp}$	S
417816	−16.32	3.68	4.44	13.43	1.22
422638	−12.45	5.76	2.16	19.3	0.65
434313	−20.11	9.9	2.03	14.69	1.37
434500	17.35	6.81	2.55	20.42	0.85
452376	9.5	3.02	3.15	12.12	0.78
465824	−28.39	10.69	2.65	29.12	0.98
469219	−59.75	17.39	3.44	91.46	0.65
474613	−14.5	6.84	2.12	17.33	0.84
489235	19.52	6.68	2.92	13.22	1.48
496816	10.39	4.6	2.26	12.42	0.84
508908	−15.77	4.85	3.25	21.9	0.72
515082	−8.2	3.38	2.43	14.79	0.55
523971	21.72	10.04	2.16	22.75	0.95
524471	23.43	9.27	2.53	17.05	1.37
526742	21.52	9.41	2.29	18.88	1.14
527977	−62.91	31.09	2.02	97.46	0.65
612027	21.72	4.71	4.61	17.65	1.23
612267	−22.13	10.44	2.12	18.26	1.21
1994 GL	368.44	58.72	6.27	251.4	1.47
1998 SL36	−21.03	7.31	2.88	14.01	1.5
1999 FN19	−28.49	13.13	2.17	26.74	1.07
2000 CR101	−14.35	5.45	2.63	11.48	1.25
2001 SQ3	−12.22	5.81	2.1	30.68	0.4
2002 LX	34.54	15.35	2.25	24.7	1.4
2005 NE21	44.84	14.16	3.17	33.48	1.34
2005 SP9	52.47	23.26	2.26	46.14	1.14
2005 WD	17.88	8.22	2.17	28.9	0.62
2006 AL4	96.94	25.66	3.78	115.6	0.84
2006 AN	−21.16	7.63	2.77	92.4	0.23
2006 NL	−24.26	11.6	2.09	19.75	1.23
2006 SY217	−34.63	12.3	2.82	24.62	1.41
2006 UL185	42.39	17.76	2.39	32.63	1.3
2006 XY	42.11	19.29	2.18	78.75	0.53
2007 DB61	−95.5	44.06	2.17	86.74	1.1
2007 TQ24	73.48	32.55	2.26	50.12	1.47
2008 GU20	22.13	8.5	2.6	40.57	0.55
2008 HA2	85.78	25.45	3.37	86.23	0.99
2008 KV2	−27.26	6.68	4.08	28.75	0.95
2008 SZ150	−92.1	29.4	3.13	74.15	1.24

Table 4 continued

Asteroid	da/dt	$\sigma_{da/dt}$	SNR	$da/dt\|_{exp}$	S
2009 FF	−13.08	5.37	2.44	29.81	0.44
2009 WC54	−116.78	41.84	2.79	99.73	1.17
2010 GC35	−37.55	14.06	2.67	97.34	0.39
2010 KP10	−37.63	9.94	3.79	45.21	0.83
2011 CE50	−74.79	24.18	3.09	53.94	1.39
2011 UC292	17.56	6.79	2.59	48.12	0.36
2011 YW10	134.64	57.19	2.35	130.92	1.03
2012 DY32	−28.61	9.23	3.1	42.08	0.68
2012 GA5	−104.58	34.74	3.01	79.81	1.31
2013 BC70	−64.91	29.27	2.22	86.44	0.75
2013 BO27	−31.76	10.36	3.06	103.04	0.31
2013 KS1	−402.04	125.79	3.2	275.39	1.46
2013 LE7	−447.61	162.0	2.76	365.85	1.22
2013 YA14	70.84	35.04	2.02	74.26	0.95
2015 EO61	60.03	26.65	2.25	42.32	1.42
2015 TW178	24.83	9.29	2.67	17.33	1.43
2015 XW261	−38.12	12.43	3.07	26.73	1.43
2016 AJ9	−53.18	19.17	2.77	82.86	0.64
2016 ED157	−39.57	15.92	2.49	93.82	0.42
2017 BN123	−51.01	24.16	2.11	49.57	1.03
2017 BP32	−44.55	12.42	3.59	52.91	0.84
2017 UJ5	−14.4	5.64	2.55	103.09	0.14
2017 XO2	−46.28	10.11	4.58	42.05	1.1
2018 CC14	43.8	13.89	3.15	37.73	1.16
2020 KP1	−46.08	15.84	2.91	44.5	1.04
2020 PP1	−145.85	49.36	2.95	263.54	0.55
2021 CF9	−28.56	12.34	2.31	22.58	1.27
2022 UY	−125.67	29.55	4.25	155.14	0.81

The columns represent, in order: the asteroid designation, the computed Yarkovsky drift and its error in $10^{-4}\ AU\ Myr^{-1}$, the SNR, the expected Yarkovsky drift in $10^{-4}\ AU\ Myr^{-1}$ and the S parameter

Author Contributions The authors contributed equally to the writing and the revision of the manuscript.

Funding Open access funding provided by Università di Pisa within the CRUI-CARE Agreement. GT acknowledges the support from the Italian Space Agency through the project "Monitoring Asteroids" (grant 2022-33-HH.0).

Availability of Data and Materials The authors declare that the data supporting the findings of this study are available within the paper and its supplementary information files.

Code Availability The data have been producted using the OrbFit software avalilable at http://adams.dm.unipi.it/orbfit/.

Declaration

Conflicts of interest The authors declare that they have no conflict of interest; the authors have no competing interests as defined by Springer, or other interests that might be perceived to influence the results and/or discussion reported in this paper.

Open Access This article is licensed under a Creative Commons Attribution 4.0 International License, which permits use, sharing, adaptation, distribution and reproduction in any medium or format, as long as you give appropriate credit to the original author(s) and the source, provide a link to the Creative Commons licence, and indicate if changes were made. The images or other third party material in this article are included in the article's Creative Commons licence, unless indicated otherwise in a credit line to the material. If material is not included in the article's Creative Commons licence and your intended use is not permitted by statutory regulation or exceeds the permitted use, you will need to obtain permission directly from the copyright holder. To view a copy of this licence, visit http://creativecommons.org/licenses/by/4.0/.

References

1. Farnocchia, D., et al.: Orbits, long-term predictions, impact monitoring. Asteroids IV, 815–834 (2015)
2. Farinella, P., Vokrouhlicky, D.: Semimajor axis mobility of asteroidal fragments. Science **283**(5407), 1507–1510 (1999)
3. Wetherill, G.W.: Steady state populations of Apollo-Amor objects. Icarus **37**(1), 96–112 (1979)
4. Wetherill, G.W.: Asteroidal source of ordinary chondrites. Meteoritics **20**(1), 1–22 (1985)
5. Wetherill, G.: Dynamical relations between asteroids, meteorites and apollo-amor objects. Philosophical Transactions of the Royal Society of London. Ser. A Math. Phys. Sci. **323**(1572), 323–337 (1987)
6. Wetherill, G.: Where do the Apollo objects come from? Icarus **76**(1), 1–18 (1988)
7. Greenberg, R., Nolan, M.C.: Delivery of asteroids and meteorites to the inner solar system. Asteroids II, 778–801 (1989)
8. Greenberg, R., Nolan, M.C.: Dynamical relationships of near-earth asteroids to main-belt asteroids. Res. Near-Earth Space 473–492 (1993)
9. Bottke, W.F., Vokrouhlicky, D., Rubincam, D.P., Broz, M.: The effect of Yarkovsky thermal forces on the dynamical evolution of asteroids and meteoroids. Asteroids III 395 (2002)
10. Bottke, W.F., Vokrouhlicky, D., Rubincam, D.P., Nesvorny, D.: The Yarkovsky and YORP effects: Implications for asteroid dynamics. Annu. Rev. Earth Planet. Sci. **34**, 157–191 (2006)
11. Öpik, E.J.: Collision probabilities with the planets and the distribution of interplanetary matter. In: Proceedings of the Royal Irish Academy. Section A: Mathematical and Physical Sciences, vol. 54, pp. 165–199. JSTOR (1951)
12. Radzievskii, V.: A mechanism for the disintegration of asteroids and meteorites. Astronomicheskii Zhurnal **29**, 162–170 (1952)
13. Rubincam, D.P.: Yarkovsky thermal drag on LAGEOS. J. Geophys. Res. **93**(B11), 13805–13810 (1988)
14. Vokrouhlicky, D., Milani, A., Chesley, S.R.: Yarkovsky effect on small near-earth asteroids: Mathematical formulation and examples. Icarus **148**(1), 118–138 (2000)
15. Chesley, S.R., et al.: Direct detection of the Yarkovsky effect by radar ranging to asteroid 6489 Golevka. Science **302**(5651), 1739–1742 (2003)
16. Chesley, S.R., et al.: Direct estimation of Yarkovsky accelerations on near-earth asteroids. LPI Contributions **1405**(8330), 37 (2008)
17. Nugent, C.R., Margot, J.L., Chesley, S.R., Vokrouhlicky, D.: Detection of semimajor axis drifts in 54 near-earth asteroids: New measurements of the Yarkovsky effect. Astron. J. **144**(2), 60 (2012)
18. Farnocchia, D., et al.: Near earth asteroids with measurable Yarkovsky effect. Icarus **224**(1), 1–13 (2013)
19. Chesley, S.R., Farnocchia, D., Pravec, P., Vokrouhlicky, D.: Direct detections of the Yarkovsky effect: Status and outlook. Proc. Int. Astron. Union **10**(S318), 250–258 (2015)
20. Del Vigna, A., et al.: Detecting the Yarkovsky effect among near-earth asteroids from astrometric data. Astron. Astrophys. **617**, 61 (2018)

21. Greenberg, A.H., et al.: Yarkovsky drift detections for 247 near-earth asteroids. Astron. J. **159**(3), 92 (2020)
22. Dziadura, K., Oszkiewicz, D., Bartczak, P.: Investigating the most promising Yarkovsky candidates using Gaia DR2 astrometry. Icarus **383**, 115040 (2022)
23. Vallenari, A., Brown, A., Prusti, T., Bruijne, J., Arenou, F., Babusiaux, C., Biermann, M., Creevey, O., Ducourant, C., Evans, D., et al.: Gaia data release 3-summary of the content and survey properties. Astron. Astrophys. **674**, 1 (2023)
24. Vokrouhlickỳ, D., Bottke, W., Chesley, S., Scheeres, D., Statler, T.: The Yarkovsky and YORP effects. Asteroids IV, 509–531 (2015)
25. Chesley, S.R., et al.: Orbit and bulk density of the OSIRIS-REx target asteroid (101955) Bennu. Icarus **235**, 5–22 (2014)
26. Milani, A., Gronchi, G.F.: Thory of Orbit Determination. Cambridge University Press (2010)
27. Park, R.S., Folkner, W.M., Williams, J.G., Boggs, D.H.: The JPL planetary and lunar ephemerides DE440 and DE441. Astron. J. **161**(3), 105 (2021)
28. Spoto, F., Milani, A., Knezevic, Z.: Asteroid family ages. Icarus **257**, 275–289 (2015)
29. Farnocchia, D., et al.: Ephemeris and hazard assessment for near-Earth asteroid (101955) Bennu based on OSIRIS-REx data. Icarus **369**, 114594 (2021)
30. Lauretta, D.S., et al.: The OSIRIS-REx target asteroid (101955) Bennu: Constraints on its physical, geological, and dynamical nature from astronomical observations. Meteorit. Planet. Sci. **50**(4), 834–849 (2015)
31. Shevchenko, V.G., et al.: Phase integral of asteroids. Astron. Astrophys. **626**, 87 (2019)
32. Milani, A., Gronchi, G.F., Knezevic, Z.: New definition of discovery for solar system objects. Earth Moon and Planets **100**(1–2), 83–116 (2007)
33. Veres, P., Farnocchia, D., Chesley, S.R., Chamberlin, A.B.: Statistical analysis of astrometric errors for the most productive asteroid surveys. Icarus **296**, 139–149 (2017)
34. Farnocchia, D., Chesley, S.R., Chamberlin, A.B., Tholen, D.J.: Star catalog position and proper motion corrections in asteroid astrometry. Icarus **245**, 94–111 (2015)
35. Warner, B.D., Harris, A.W., Pravec, P.: The asteroid lightcurve database. Icarus **202**(1), 134–146 (2009)
36. Vokrouhlickỳ, D., Farnocchia, D., Čapek, D., Chesley, S.R., Pravec, P., Scheirich, P., Müller, T.G.: The Yarkovsky effect for 99942 Apophis. Icarus **252**, 277–283 (2015)
37. Tholen, D., Farnocchia, D.: Detection of Yarkovsky acceleration of (99942) Apophis. In: AAS/Division for Planetary Sciences Meeting Abstracts, vol. 52, pp. 214–06 (2020)
38. Pérez-Hernández, J.A., Benet, L.: Non-zero Yarkovsky acceleration for near-earth asteroid (99942) Apophis. Commun. Earth Environ. **3**(1), 10 (2022)
39. Vokrouhlickỳ, D., Čapek, D., Chesley, S., Ostro, S.: Yarkovsky detection opportunities. I. solitary asteroids. Icarus **173**(1), 166–184 (2005)
40. Mommert, M., et al.: Constraining the physical properties of near-Earth object 2009 BD. Astrophys. J. **786**(2), 148 (2014)
41. Vokrouhlicky, D., Capek, D., Chesley, S.R., Ostro, S.J.: Yarkovsky detection opportunities: II. binary systems. Icarus **179**(1), 128–138 (2005)
42. La Spina, A., Paolicchi, P., Kryszczynska, A., Pravec, P.: Retrograde spins of near-Earth asteroids from the Yarkovsky effect. Nature **428**(6981), 400–401 (2004)
43. Delbo, M., Dell"Oro, A., Harris, A.W., Mottola, S., Mueller, M.: Thermal inertia of near-Earth asteroids and implications for the magnitude of the Yarkovsky effect. Icarus **190**(1), 236–249 (2007)
44. Michel, P., et al.: The ESA Hera Mission: Detailed characterization of the DART impact outcome and of the binary asteroid (65803) Didymos. The Planet. Sci. J. **3**(7), 160 (2022)

Publisher's Note Springer Nature remains neutral with regard to jurisdictional claims in published maps and institutional affiliations.